Journal of Materials Chemistry B

ROYAL SOCIETY OF CHEMISTRY

PAPER

View Article Online
View Journal | View Issue

Cite this: J. Mater. Chem. B, 2022, 10, 2680

Short-wave and near infrared π-conjugated polymers hosted in a biocompatible microemulsion: a pioneering approach for photoacoustic contrast agents

Evgenia Mitsou,†[a] Ioanna Theochari,†[a] Evdokia Vassiliadi,[ab] Frédéric Nallet[c] and Aristotelis Xenakis *[a]

Received 16th October 2021,
Accepted 19th December 2021

DOI: 10.1039/d1tb02257a

rsc.li/materials-b

In the present study a biocompatible oil-in-water (O/W) microemulsion was developed carrying short-wave infrared (SWIR) π-conjugated polymers and possessing photoacoustic properties for the first time. SWIR and NIR absorbing conjugated polymers were accomplished to be dissolved in a Food & Drug Administration (FDA) approved natural oil limonene, to formulate an O/W microemulsion using biocompatible surfactants (Span80, Labrasol®). Detailed structural characterization in the absence and presence of the polymers was performed by means of dynamic light scattering (DLS), small-angle X-ray scattering (SAXS) and electron paramagnetic resonance (EPR) spectroscopy. In terms of biological evaluation of the loaded microemulsions, inhibition of cell proliferation in various cancer cell lines without exhibiting significant cytotoxicity was tested through the MTT assay. The developed π-conjugated polymers hosted in O/W microemulsions represent a technological approach with a wide range of biomedical and bioelectronic applications and in this contribution, their photoacoustic properties are presented as a proof-of-concept.

1. Introduction

Biological imaging in the near infrared (NIR) and especially in the short wavelength infrared region (SWIR) has shown remarkable potential of overcoming various issues associated with the conventional optical bioimaging applications.[1–4] This is because at progressively longer wavelengths beyond 1000 nm, the absorption and scattering of photons by biological moieties are minimal, yielding significantly deeper imaging penetration depths, enhanced spatial resolution, improved imaging fidelity, and minimized background autofluorescence. Understandably, recent activities have been focused on the design and development of novel exogenous imaging contrast agents with absorption or emission above 1000 nm and with the capability to generate strong SWIR photoacoustic or fluorescence signals for optical bioimaging in the spectral region from 1000 to 1700 nm. π-Conjugated polymers especially in the form of nanoparticles, the so-called conjugated polymer nanoparticles (CPNs), have emerged as powerful nanomaterials for optical (fluorescent and/or photoacoustic) bioimaging applications in the SWIR region.[5,6] This is due to the fact that their optoelectronic properties can be easily tuned to the SWIR region through facile chemical design and synthesis by using completely benign and biologically inert components.

Two main strategies have been developed to address the insolubility of conjugated polymers in polar solvents. These include the post-polymerization methods and the direct polymerization techniques in disperse hetero-phase systems.[7] In post-polymerization techniques, the conjugated polymer is first prepared in a non-polar medium, which is a good solvent for the resulting conjugated polymer. These conjugated polymers are then "shaped" into colloidal particles *via* nanoprecipitation, encapsulation or functionalization with hydrophilic groups.[8] As a result, conjugated polymer nanoparticles (CPNs) can be generated from commercially available and purified polymers by dispersion in a polar non-solvent. By contrast, in direct polymerization techniques the CPNs are generated *in situ* during polymer synthesis. Dispersion polymerization and polymerization in so-called miniemulsion are established methods for the preparation of CPNs.[9,10] While direct polymerization techniques offer better control over the shape and dispersity of the particles, the post-polymerization techniques are more flexible in terms of the type of the conjugated polymer materials and their purity, as these are prepared in a stand-alone and separate reaction step, which allows for intermediate purification steps. In this work, a new

[a] Institute of Chemical Biology, National Hellenic Research Foundation, 48 Vassileos Constantinou Avenue, Athens, 11635, Greece. E-mail: arisx@eie.gr
[b] Biotechnology Laboratory, Department of Biological Applications and Technologies, University of Ioannina, 45110 Ioannina, Greece
[c] Centre de Recherche Paul Pascal – CNRS, University of Bordeaux, 33600 Pessac, France
† Equal contribution.

methodology is described for the preparation of biocompatible soft nanocarriers containing SWIR and NIR absorbing conjugated polymers which maintain the flexibility of the post-polymerization techniques and offer better control over the shape and dispersity index of the particles of polymerization in miniemulsion.

Among soft nanocarriers, liquid nanodispersions and especially microemulsions possess unique properties due to their physicochemical behavior. Microemulsions are optically isotropic, liquid systems consisting of water, oil and amphiphilic compounds. Moreover, they are formed spontaneously and are thermodynamically stable and for that reason should not be confused with the aforementioned miniemulsions.[11] In more detail, microemulsions remain stable indefinitely provided the initial conditions remain unaltered. Microemulsions are characterized by optical clarity due to their small droplet size that ranges between 5 and 50 nm. This type of nanocarrier is classified into three categories: water-in-oil (W/O), oil-in-water (O/W) and bicontinuous ones.[12,13] Owing to their small size, microemulsions are able to penetrate biological barriers while offering protection to the encapsulated substance against chemical and/or enzymatic degradation.[14] Microemulsions have been the center of interest in the last few decades for medical applications, not only because of their stability, but also because of their low viscosity and the ease of preparation. For these reasons, microemulsions could be suitable carriers of conjugated polymers for potential visualization of tissues. To the best of our knowledge, microemulsions were proposed to encapsulate fluorescent probes, detectable in the visible or UV region up to now, but there is no study related to microemulsions as proposed nanocarriers for conjugated polymers possessing photoacoustic and photothermal properties.[15,16]

In order to fully exploit the applicability of O/W microemulsions, biocompatible, non-ionic systems with encapsulated NIR and SWIR conjugated polymers were developed. The main aim of the study was the effective incorporation of the conjugated polymers in the dispersed phase of a microemulsion to enhance their aqueous solubility without affecting their optoelectronic properties and applications (*e.g.* photoacoustic). The soft nanodispersions were developed and characterized both for their physicochemical behavior and for their *in vitro* toxicity. Towards this approach, non-ionic surfactants are the most appropriate for biomedical applications in terms of irritancy and toxicity.[17] In this respect, biocompatible and non-toxic O/W microemulsions were prepared comprising of non-ionic surfactants (Span 80, Labrasol®) and an FDA approved essential oil (limonene) to encapsulate the synthesized NIR PBDT-DPP and SWIR PIDT-TDQ polymers. As a proof of concept, the study presents the promising potential of these biocompatible systems with incorporated conjugated polymers to serve as new photoacoustic contrast agents.

2. Materials and methods

2.1 Materials

All reactions, regarding the synthesis of the conjugated polymers, are air and light sensitive and, therefore, were performed under argon and in the dark. All glassware was washed using detergent (Teepol), rinsed with excess water, acetone and methylene dichloride and dried in an oven at 120 °C. All solvents and reagents were purchased from Aldrich. Toluene was distilled using calcium hydride (CaH_2) and benzophenone prior to polymerization. The synthesis of the polymers was performed using the commercially available (4,4,9,9-tetrakis(4-hexylphenyl)-4,9-dihydro-*s*-indaceno[1,2-*b*:5,6-*b*′]dithiophene-2,7-diyl)bis(trimethylstannane), (4,8-bis(5-(2-ethylhexyl)thiophen-2-yl)benzo[1,2-*b*:4,5-*b*′]dithiophene-2,6-diyl) bis(trimethylstannane), 4,9-dibromo-6,7-diphenyl-[1,2,5]thiadiazolo[3,4-*g*]quinoxaline and 3,6-bis(5-bromothiophen-2-yl)-2,5-bis(2-butyloctyl)-2,5-dihydropyrrolo[3,4-*c*]pyrrole-1,4-dione according to already published procedures.[18–21] *R*-(+)-Limonene (97%) and Sorbitan monooleate (Span 80) were provided by Thermo Fisher Scientific (Karlsruhe, Germany). Labrasol® ALF was kindly donated by Gattefossé (Cedex, France). 5-Doxyl stearic acid (5-DSA), 16-Doxyl stearic acid (16-DSA), tris(dibenzylideneacetone)dipalladium(0) [$Pd_2(dba)_3$] and tri(*o*-tolyl)phosphine [$P(o\text{-tol})_3$] were purchased from Sigma-Aldrich (Munich, Germany). High-purity water was obtained from a Millipore Milli-Q Plus water purification system.

2.2 Synthesis of conjugated polymers

Synthesis of PIDT-TDQ. (4,4,9,9-Tetrakis(4-hexylphenyl)-4,9-dihydro-*s*-indaceno[1,2-*b*:5,6-*b*′]dithiophene-2,7-diyl)bis(trimethylstannane) (0.5 mmol) was combined with 4,9-dibromo-6,7-diphenyl-[1,2,5]thiadiazolo[3,4-*g*]quinoxaline (0.5 mmol) and dry toluene (0.025 M) was added to the reaction mixture. Finally, tris(dibenzylideneacetone)dipalladium(0) [$Pd_2(dba_3)$] (0.02 equiv.) and tri(*o*-tolyl)phosphine [$P(o\text{-tol})_3$] (0.08 equiv.) were added and the reaction mixture was stirred at 120 °C under an argon atmosphere for 24 h. The crude polymer was purified by precipitation in methanol, filtered and washed using a Soxhlet apparatus with methanol, acetone, hexane and chloroform. The chloroform fraction was evaporated under reduced pressure and the polymer precipitated in methanol, filtered through 0.45 mm PTFE filter and finally dried under high vacuum, rendering a dark solid. The yield of the resulting polymer is 88%. PIDT-TDQ; ^{1}H NMR ($CDCl_3$, 600 MHz) δ 7.78 (s, 4H), 7.58 (s, 1H), 7.35 (d, 2H), 7.12 (b, 4H), 2.58 (b, 2H), 1.61 (d, 2H), 1.27 (d, 6H), 0.85 (s, 3H) SEC ($CDCl_3$): M_n = 133 000 g mol^{-1}, $Đ$ = 1.85.

Synthesis of PBDT-DPP. A similar procedure and purification were followed for the synthesis of PBDT–DPP except that (4,8-bis(5-(2-ethylhexyl)thiophen-2-yl)benzo[1,2-*b*:4,5-*b*′]dithiophene-2,6-diyl)bis (trimethylstannane) (0.5 mmol) and 3,6-bis(5-bromothiophen-2-yl)-2,5-bis(2-butyloctyl)-2,5-dihydropyrrolo[3,4-*c*]pyrrole-1,4-dione (0.5 mmol) were used as precursor monomers. The yield of the resulting polymer is 74%. PBDT–DPP; ^{1}H NMR ($CDCl_3$, 600 MHz) δ 7.8 (b, 1H), 7.33 (b, 1H), 7.48–6.95 (m, 5H), 6.90–6.71 (d, 1H), 3.91–3.42 (b, 2H), 1.66–0.92 (m, 12H), 0.91–0.74 (m, 3H), SEC ($CDCl_3$): M_n = 19 900 g mol^{-1}, $Đ$ = 3.2.

2.3 Formulation of microemulsions

O/W microemulsions consisting of limonene as the oil phase, distilled water as the aqueous phase, and Labrasol® and Span 80 as surfactants were formulated for the encapsulation of the synthesized polymers. A pseudo-ternary phase diagram was constructed in order to investigate the phase behavior of the

system.[22] In more detail, mixtures of water/surfactants were prepared by altering the mass ratios from 9 : 1 to 1 : 9. The dispersed oil phase was added dropwise as long as the samples remained transparent. During titration, samples were left to equilibrate from few minutes up to 24 h at constant temperature (25 °C). The results were visualized using the ProSim Ternary Diagram software and the monophasic region of microemulsions was determined. The composition of the microemulsion chosen for further investigation was 78.7 wt% water, 17.5 wt% surfactants (Labrasol® to Span 80 ratio was 8.7 : 1) and 3.8 wt% limonene.

2.4 Encapsulation of PBDT-DPP and PIDT-TDQ

PBDT-DPP and PIDT-TDQ were dissolved in limonene prior to emulsification. Solutions of PBDT-DPP and PIDT-TDQ were left in an ultrasound water bath for 2 h at 45 °C. The solubility of the two conjugated polymers was different in the chosen oil: 0.04 mg mL^{-1} for PBDT-DPP and 0.21 mg mL^{-1} for PIDT-TDQ. Limonene polymer saturated solutions were used as the oil phase for the loaded microemulsions and the final concentrations of the polymers were calculated to be 1.5 μg mL^{-1} for PBDT-DPP and 7.9 μg mL^{-1} for PIDT-TDQ.

2.5 Nuclear magnetic resonance (NMR)

^{1}H-NMR measurements were carried out in solutions (1% w/v) of the copolymers using $CDCl_3$ (Acros 99.6%) as the solvent and tetramethylsilane (TMS) as the integral standard on a Varian 600 MHz NMR spectrometer at ambient temperature.

2.6 Gel permeation chromatography (GPC)

Average molecular weights per number ($\overline{M_n}$) and polydispersity indices ($Đ$) were determined by GPC at 80 °C on a Shimadzu liquid chromatograph (LC-20AD) system consisting of a DGU-20A5R degassing unit, a SIL-20AC HT auto sampler, a CTO-20AC column oven, a SPD-20AV UV-Vis detector and a RID-20A refractive index detector connected in series. The system contains a PL-GEL 10 μm guard column, two PL-GEL 10 μm mixed-B columns and chlorobenzene (CB) as the eluent. The instrument was calibrated with narrow polystyrene standards with M_p ranging from 4730 g mol^{-1} to 3 187 000 g mol^{-1}.

2.7 Dynamic light scattering (DLS)

Structural study was performed using dynamic light scattering (DLS) in order to determine the mean diameter (d, nm) of nanodroplets and the polydispersity index (PdI) of the system. DLS measurements were performed using the Zetasizer NanoZS device (ZEN3600) from Malvern Instruments (UK) equipped with a He–Ne (632.8 nm) laser and detection was performed at a scattering angle of 173°. The mean diameter (d) of the dispersed nanodroplets was calculated by the Stokes–Einstein law:

$$R_H = \left(\frac{k_B T}{6\pi\eta d}\right) \quad (1)$$

where R_H is the hydrodynamic radius of nanodroplets, k_B is the Boltzmann constant, T is the absolute temperature, η is the viscosity of the microemulsion (at a specific temperature) and D is the diffusion constant.[23]

After their preparation the microemulsions were placed in a suitable glass cell in dust-free conditions. The experimental data were processed using version 6.32 of the Malvern Zetasizer Nano software (Malvern Panalytical Ltd, Enigma Business Park, UK). Microemulsions were measured in the absence (empty) and presence (loaded) of conjugated polymers. The temperature during the measurements was constant at either 25 °C (storage temperature) or 37 °C (temperature of *in vitro* assays). Experiments were performed in triplicate for each sample, and results were presented as average ± S.D.

2.8 Electron paramagnetic resonance (EPR) spectroscopy

The interfacial properties of the biocompatible O/W microemulsions in the absence and in the presence of the conjugated polymers were studied with the use of electron paramagnetic resonance (EPR) spectroscopy applying the spin-probing approach.[24] Two widely used spin-probes of amphiphilic nature were employed, namely 5-doxyl stearic acid (5-DSA) and 16-doxyl stearic acid (16-DSA). These interface-located fatty acid spin probes give EPR spectra reflecting the rigidity/flexibility of their environment on the depth of the membrane where their paramagnetic moiety is located, as reported previously.[25] Measurements were performed using a Bruker EMX EPR spectrometer operating at the X-band (9.8 GHz). Samples were placed in a quartz flat cell by Wilmad (Buena, NJ). The parameters used for the experimental procedure were center field 0.349 T, scan range 0.01 T, receiver gain 5.64 × 10^3, time constant 5.12 ms, conversion time 5 ms, modulation amplitude 0.4 mT, and frequency 9.78 GHz. The final spin-probe concentration in the microemulsions was 10^{-4} M. The spin-probes were initially dissolved in an ethanolic stock solution, which was deposited in Eppendorf tubes and then evaporated to receive later the microemulsions. Prior to evaporation, 1 mL of each system was deposited and left at 25 °C overnight to reach equilibrium. Data collection and analysis were performed using the Bruker WinEPR acquisition and processing programs. Experimental results were analyzed in terms of rotational correlation time (τ_R), order parameter (S) and isotropic hyperfine splitting constant (A_o). The equations regarding the calculations of the described parameters have been thoroughly described previously.[26] It has to be underlined that in the present study, as the τ_R values of all the systems belong to the fast motion region ($\tau_R < 3$ ns) all the parameters were calculated from the experimental data without the use of computer simulations.

2.9 Small angle X-ray scattering (SAXS)

Small angle X-ray scattering (SAXS) experiments, for microemulsions in the presence and absence of the conjugated polymers, were carried out on a XEUSS 2.0 device (XENOCS, Grenoble, France). Coupled to a FOX3D single reflection optical mirror centered on the Cu K_α radiation (λ = 1.54 Å), the GeniX3D source delivers a 8 keV beam which is further collimated by a set of 2 motorized scatter-less slits. The samples were put in thin glass capillaries (optical path 2 mm) and

exposed for 3 hours. The data were collected using a two-dimensional PILATUS-300k detector (DECTRIS, Baden-Dättwill, Switzerland) placed perpendicularly to the direct beam at a distance of 1634 mm, calibrated with a silver behenate standard. Images with a size of 487 × 619 pixels (hor. × vert., pixel size 172 μm) were obtained, giving access to a range of scattering wave vectors q from typically 0.006 A^{-1} to 0.24 A^{-1} in the chosen configuration where the direct beam is approximately horizontally centered, but located vertically about one-sixth above the lower edge of the detector. The 1D diffractograms (intensity I *vs.* q) have been obtained by processing the raw detector images with the FOXTROT software (collaboration between XENOCS and the SOLEIL synchrotron (Gif-sur-Yvette, FRANCE) SWING beamline team).

2.10 Viscosity measurements

Viscosity measurements of the microemulsions were performed at a shear rate of 50 rpm, using a DV-I Prime Digital Viscometer (Brookfield Engineering Laboratories, USA), equipped with core spindle (CPA-40Z). The temperature was kept constant at either 25 °C or 37 °C using a water bath. Experiments were performed in triplicate for each sample (empty and loaded), and results were presented as average ± S.D.

2.11 Cell lines

The cell line RPMI 2650 (CCL-30) was kindly provided by Dr Fabio Sonvico (University of Parma, Italy). The human melanoma cell line WM 164 (BRAFV600E, p53Y220C; Wistar Institute Melanoma Research Centre, https://wistar.org/) was generously provided by Dr G. Skretas (National Hellenic Research Foundation, Athens, Greece). The human liver cancer cell line (Hep-G2), human colon cancer cell line (HTC 116) and human prostate cancer cell line (PC-3) were purchased from the American Type Culture Collection (ATCC, Manassas, VA, USA). All cell lines, except RPMI 2650, were grown in Dulbecco's modified Eagle's medium (DMEM) containing 4.5 g L^{-1} glucose, L-glutamine and pyruvate, supplemented with 10% fetal bovine serum (FBS) and 1% penicillin/streptomycin (Gibco-Life Technologies, Grand Island, NY, USA), at 37 °C in a humidified incubator with 5% CO_2. The RPMI 2650 cells were grown in minimum essential medium (MEM) containing 4.5 g L^{-1} glucose, L-glutamine and pyruvate, supplemented with 10% FBS and 1% penicillin/streptomycin. All cell culture plasticware was supplied by Corning Costar (Lowell, MA, USA). Trypsin 0.25% and phosphate-buffered saline (PBS) were purchased from Gibco-Life Technologies (Grand Island, NY, USA) and dimethyl sulfoxide (DMSO) suitable for cell culture and thiazolyl blue tetrazolium bromide (MTT) were obtained from Sigma-Aldrich (Munich, Germany).

2.12 *In vitro* cell viability assay

Cells were grown in monolayers either in DMEM or in MEM as described in the previous section. When confluency reached almost 70%, cells were detached from the culture area by trypsinization. Initially, the cells were rinsed with PBS buffer and then trypsin solution was added (0.25% wt in EDTA). Cells were placed in 96-well plates at a density of 5–10 × 10^3 cells per well, depending on the cell line used, and were allowed to adhere in medium for 24 h. Then, the medium was removed and replaced with a fresh one, containing empty and loaded microemulsions at concentrations of 0.1% v/v, 0.2% v/v, 0.5% v/v and 1% v/v in the culture medium. Inhibition of cell proliferation was assessed for 72 h after treatment with microemulsions by the MTT assay according to the manufacturer's standard protocol (M5655; Sigma-Aldrich). In brief, stock solution of the dye (5 mg mL^{-1}) was added to each culture being assayed to equal one-tenth of the original culture volume and incubated for 3 h. After the incubation period the solution was removed and replaced with a solution of isopropanol : DMSO (1 : 1) in order to dilute the insoluble purple formazan crystals. The absorbance of the converted dye was measured at 570 nm. In order to determine cell viability, eqn (2) was used:

$$\text{Cell viability } (\%) = \frac{(\text{OD of treated cells})}{(\text{OD of control})} \times 100 \qquad (2)$$

where OD is the optical density.

2.13 Photoacoustic properties

In order to study the photoacoustic signal of PBDT-DPP and PIDT-TDQ a commercially available phantom test which consisted of transparent capillary tubes was used for sample characterization. The tubes were mounted on an acrylic dish filled with distilled water for better coupling of the generated sound signals. The microemulsions containing the conjugated polymers were injected into the capillary tubing and the system acquired a sequence of photoacoustic signals in the wavelength range of 680–970 nm with a step size of 5 nm in the spectral mode. After acquisition, the images were analyzed using Vevo LAB software (FUJIFILM Visualsonics, The Netherlands) and the spectral characteristics of the samples were recorded.

3. Results and discussion

3.1 Synthesis and optical properties of PBDT-DPP and PIDT-TDQ

A fine way to tune the properties of π-conjugated polymers is the covalent coupling of at least one electron donating (D) unit to at least one electron deficient (A) unit, directly or through a π-conjugated linkage.[27] Although many different structural design strategies have been developed, the donor–acceptor (D–A) and donor–π spacer–acceptor–π spacer (D–π–A–π) approaches are the most popular and efficient methods in the literature for lowering the optical band gap. In this contribution, our aim is to develop NIR and SWIR conjugated polymers based on the D–A and D–π–A–π motifs.

In particular, we will employ the chemical design concept of the combination of a ''strong'' A, such as diketopyrrolopyrrole (DPP) or thiadiazoloquinoxaline (TDQ), with a ''moderate'' D, including benzodithiophene (BDT) or indacenodithiophene (IDT), which results in strong intramolecular charge transfer (ICT) and as a consequence in the red shift of the absorption spectrum into the NIR and SWIR.[27] We chose the DPP and TDQ monomers for the synthesis of the conjugated polymers because they have proven efficient in the development of low

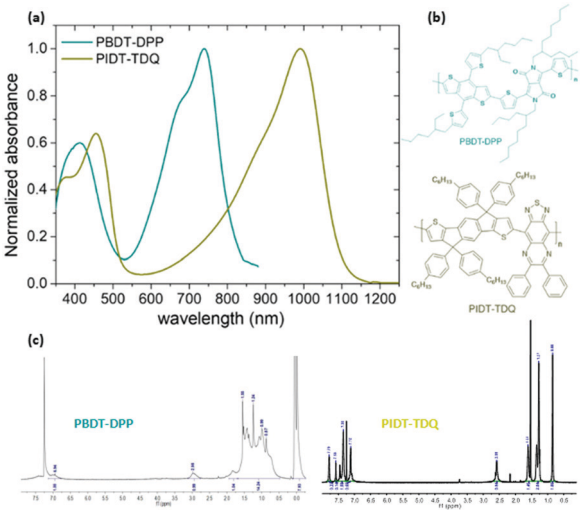

Fig. 1 (a) Absorption spectra of the conjugated polymers PBDT-DPP and PIDT-TDQ in tetrahydrofuran (THF), (b) chemical structures and their corresponding (c) ^{1}H NMR spectra.

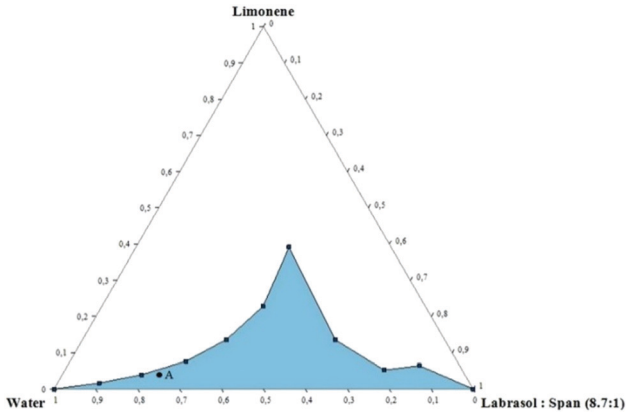

Fig. 2 Pseudo-ternary phase diagram of the system consisting of limonene as the oil phase, Labrasol® and Span 80 as surfactants and distilled water as the continuous phase. Composition is in weight ratios. The monophasic region of the system is shaded with blue color and clear area is the multi-phase region. Point A corresponds to the following composition: 78.7% water, 17.5% surfactants and 3.8% limonene. Temperature was kept constant at 25 °C.

bandgap conjugated polymers.[28] In order to obtain an easily solution processable conjugated polymer, positioning of alkyl side chains onto the polymeric backbone was included. Two conjugated polymers namely PBDT-DPP and PIDT-TDQ were synthesized based on the Stille cross-coupling polymerization procedure[29] (Fig. 1). PBDT-DPP consists of a BDT derivative and a DPP unit linked in the D–π–A–π motif, while PIDT-TDQ consists of an IDT as the electron donating (D) and a TDQ as the electron withdrawing (A) moiety. The absorption spectra of PBDT-DPP and PIDT-TDQ in tetrahydrofuran (THF) solution are presented in Fig. 1. All polymers display a qualitatively similar spectral shape. For each polymer, two major absorption bands are observed in solution. PBDT-DPP is a NIR absorbing polymer with the maximum absorption at 740 nm in tetrahydrofuran (THF) solution, while PIDT-TDQ is a SWIR absorbing polymer with the maximum absorption at 990 nm in THF solution.

3.2 Formulation of microemulsions

Pseudo-ternary phase diagrams are useful tools to investigate the phase behavior of the composed systems. A typical phase diagram is illustrated by an equilateral triangle with each vertex corresponding to an individual component or mixture of components at a constant ratio. Each point in the inner area of the triangle represents a well-defined mixture of all components in a certain ratio. The single-phase region (colored region) corresponds to clear and transparent microemulsions. Fig. 2 represents the pseudo-ternary phase diagram of distilled water, Labrasol®, Span 80 and limonene.

As it can be observed, the increase of surfactant concentration up to 60% in the overall system led to an increase of oil content and as a result, the monophasic area was expanded in terms of boundaries. Interestingly, the system corresponding to the 4 : 6 water : surfactant ratio is able to incorporate increased limonene concentration. This led to a progressive transition from an O/W to a W/O system where the oil content is higher than the aqueous phase. Those systems are called U-type systems and have been studied extensively.[30] Shorter aliphatic chain alcohols such as propylene glycol and others are known to facilitate the formation of U-type systems; however, in the current study, no co-solvents or co-surfactants have been added.

In the present case we did not focus on this specific ratio as a high concentration of surfactants would be a hurdle for the biocompatibility of the system. However, a U-type system such as the present one could be used in other applications in order to encapsulate simultaneously compounds of different polarities.

Moreover, stable and transparent microemulsions were obtained for all mass ratios of water/Labrasol®-Span 80 tested. Even at low surfactant concentrations, significant amounts of oil were successfully dispersed in the aqueous phase. For this reason, a microemulsion with low surfactant content was chosen for further investigation, taking into consideration its potential medical application. The selected system was composed of 78.7 wt% water, 17.5 wt% surfactants and 3.8 wt% limonene (Point A).

3.3 Dynamic light scattering (DLS)

The hydrodynamic diameter of nanodroplets was determined in the selected system in the absence and presence of PBDT-DPP and PIDT-TDQ, both at storage temperature (25 °C) and at the temperature of *in vitro* applications (37 °C). DLS was used in order to evaluate both the size and the polydispersity of the dispersed oil droplets of the microemulsions (Table 1). When the loaded microemulsions were measured at 25 °C, the size of nanodroplets changed significantly with the encapsulation of PIDT–DPP, but this phenomenon was not observed with the encapsulation of PBDT–TDQ. In particular, the diameter of nanodroplets was increased by approximately 8 nm after the encapsulation of PIDT–DPP which could be correlated with the increased concentration of the polymer in the dispersed phase

Table 1 Apparent hydrodynamic diameter (nm) and polydispersity index (PdI) of empty and loaded microemulsions at 25 °C and 37 °C

	Empty		Loaded PBDT-DPP		Loaded PIDT-TDQ	
Temperature (°C)	d (nm)	PdI	d (nm)	PdI	d (nm)	PdI
25	10.2 ± 0.1	0.21 ± 0.01	10.3 ± 0.1	0.23 ± 0.01	17.8 ± 0.3	0.23 ± 0.02
37	18.5 ± 1.4	0.22 ± 0.01	19.9 ± 1.9	0.20 ± 0.01	79.4 ± 5.6	0.11 ± 0.01

and also its structure. In the case of microemulsion loaded with PBDT–TDQ, the diameter of nanodroplets was not affected upon encapsulation compared to the empty sample. As the concentration of PBDT–TDQ was lower, compared to PIDT–DPP, it seems that the concentration of the encapsulated compound affects the size of nanodroplets. It has to be underlined that in the present study the highest encapsulation concentrations were used in order to formulate an effective final carrier for photoacoustic properties. The polydispersity index (PdI) did not differ after π-conjugated polymer encapsulation in the case of measurement at 25 °C and remained at low values (PdI $<$ 0.4).

When the samples were measured at 37 °C, the mean diameter of nanodroplets in all cases was increased, indicating that the increase of temperature affected the size. Especially in the case of PIDT-TDQ the increase of the diameter is reflected in the presence of a slight turbid appearance. According to the literature, temperature may have an effect on self-assembled colloidal structures including microemulsions. This is primarily attributed to the surfactant molecules as it is known that the critical micelle concentration (CMC) depends on temperature.[31] Also, in the case of non-ionic microemulsions the spontaneous curvature can be controlled simply by altering the temperature as Lindman *et al.* have reported.[32] Experimental data have proven that temperature alterations affect non-ionic microemulsions mostly due to the temperature dependency of the hydrophobic effect and the interactions between non-polar and polar components.[31,33,34] The drastic increase of the nanodroplet size of PIDT-TDQ loaded microemulsions and the subsequent decrease of the PdI value are linked. The increase of temperature induces an increase in the diameter of the micelles due to the addition of the high concentration of the polymer.

3.4 Electron paramagnetic resonance (EPR) spectroscopy

Interfacial properties and polarity of the monolayer of surfactants between the dispersed and continuous phase of nanodroplets were investigated by performing EPR spectroscopy with the use of appropriate spin-probes. For this purpose, an amphiphilic probe, possessing unpaired electrons, was incorporated into the sample at a given concentration. In this study, 5-doxyl stearic acid (5-DSA) and 16-doxyl stearic acid (16-DSA) were used as amphiphilic spin-probes. Both molecules consist of a stearic acid and a doxyl group in C-5 and C-16 positions in the carbon chain respectively and are localized at the surfactant monolayer.

It has to be underlined that in the case of 5-DSA, the doxyl group is aligned closer to the polar head, whereas in the case of 16-DSA the doxyl group is aligned closer to non-polar tails. The obtained EPR spectra are affected by amphiphile environment, depending on the depth of the membrane where the doxyl group is located. Thus, any change in spectra can be associated with structural alterations of the surfactant monolayer reflecting the rigidity/flexibility on this specific depth. To obtain the above information, several parameters were calculated through the obtained probe's spectra: namely, (a) rotational correlation time of the spin-probe (τ_R), (b) order parameter (S) and (c) isotropic hyperfine splitting constant (A_0).[24] τ_R is a parameter that gives information about the mobility of the spin-probe and represents the time that the spin-probe needs in order to make a full rotation. Order parameter S provides a measure of the spin-probe's arrangement in a supramolecular assembly while A_0 is a parameter that indicates the micropolarity near the doxyl group of the probe.[26,35–37]

All these parameters were calculated from the spectra and are given in Table 2. Experiments were performed in triplicate and the results are expressed as mean values ± standard deviation (SD).

Fig. 3 shows the experimental EPR spectra of 5-DSA and 16-DSA in empty and loaded microemulsions. A_0 as indicated in

Table 2 Rotational correlation time (τ_R), order parameter (S) and isotropic hyperfine splitting constant (A_0) of 5-DSA and 16-DSA in empty and loaded microemulsions

5-DSA	τ_R (ns)	S	A_0
Empty	2.16 ± 0.03	0.10 ± 0.01	14.06 ± 0.05
Loaded PBDT-DPP	2.18 ± 0.03	0.10 ± 0.01	14.01 ± 0.04
Loaded PIDT-TDQ	2.11 ± 0.12	0.11 ± 0.01	14.12 ± 0.14
16-DSA			
Empty	0.26 ± 0.01	0.03 ± 0.01	14.80 ± 0.01
Loaded PBDT-DPP	0.25 ± 0.01	0.03 ± 0.01	14.78 ± 0.02
Loaded PIDT-TDQ	0.24 ± 0.01	0.03 ± 0.01	14.79 ± 0.02

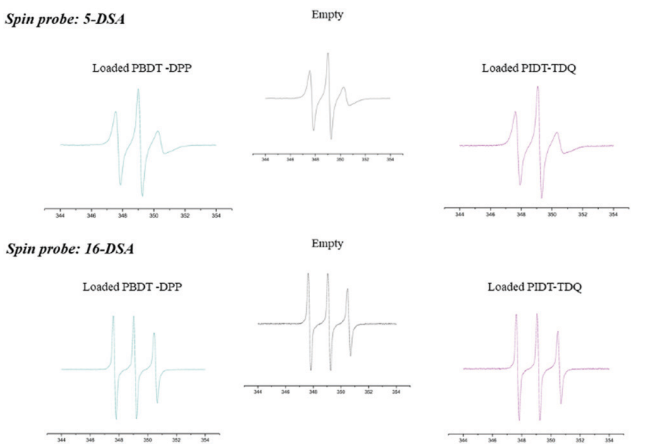

Fig. 3 EPR spectra of 5-DSA and 16-DSA in the empty O/W system and the one loaded with PBDT-DPP and PIDT-TDQ polymers.

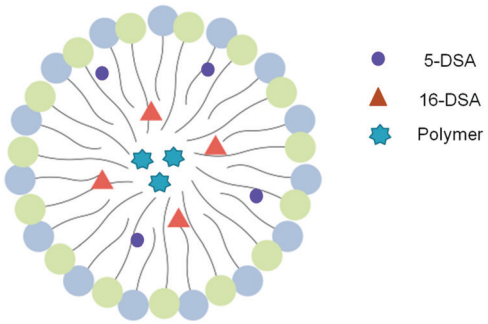

Fig. 4 Schematic representation of the localization of spin probes and polymer molecules in an oil droplet of the O/W microemulsion based on EPR results.

Table 2 does not significantly change upon the addition of the polymers in both cases meaning that the recognizable environmental polarity is primarily the same. It has to be mentioned that the fact that the A_0 of 5-DSA in the systems is lower than that of 16-DSA was not expected but it can be explained in accordance with the structure of the system and the distribution of Labrasol between the aqueous and oil phases. The data indicated that the addition of both PBDT-DPP and PIDT-TDQ in the microemulsions did not affect the calculated parameters since no significant alterations in the spectra were observed. Moreover, π-conjugated polymers are located within the oily cores of the microemulsions and not interacting with the surfactant layer at any depth (Fig. 4). Microemulsions are characterized by low order parameter values in the case of 16-DSA, which indicates a less restricted movement of the spin-probes in the inner part of the membrane in comparison with its outer part. In general, the degree of rigidity of the membrane has been related to the permeability and bioavailability of the encapsulated compounds.[38] Parameter S in both cases is low indicating a relatively flexible environment in which the encapsulated compounds are more free to move and to be released from the systems.

3.5 Small angle X-ray scattering (SAXS)

SAXS is an analytical and non-destructive method to investigate nanostructures in liquids and solids. SAXS is able to probe the colloidal length scales of 10–1000 Å and therefore is an appropriate method to determine the size and the structure of colloidal systems such as microemulsions. In the present study, this method was used in order to clarify the possible alterations that may be produced in the nanodispersion's structure after the incorporation of the two polymers in the dispersed phase. Fig. 5 represents the intensity profile of microemulsions in the absence (blue line) and presence (green and red curve) of PBDT-DPP and PIDT-TDQ polymers respectively, with the usual "microemulsion peak"[39] characteristic of spatial correlations between oil droplets. Note that this peak precludes a Guinier analysis of the scattering intensity in the small q limit. Interestingly, SAXS profiles for the empty system and the PBDT-DPP loaded system are nearly symmetric and broadly similar in the investigated q range, with peak location q^* = 0.052 Å^{-1} and

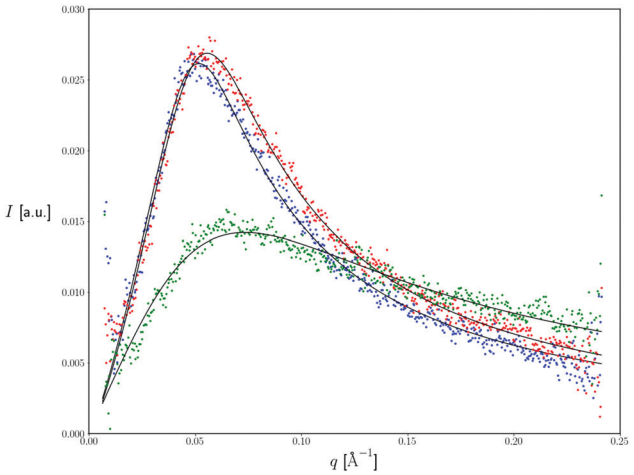

Fig. 5 SAXS spectra of the empty microemulsion (blue line) and that loaded with the conjugated polymers (red line – microemulsion with PBDT-DPP, green line – microemulsion with PIDT-TDQ). Lower panel: Processed data, subtracting the buffer contribution. Linear scale. Continuous black lines: best fits. Measuring temperature: 25 °C.

0.056 Å^{-1} and half-width at half-maximum 0.027 Å^{-1} and 0.030 Å^{-1}, respectively. In contrast, the profile of the PIDT-TDQ loaded system is extremely different in both peak position (q^* = 0.074 Å^{-1}) and peak width (*ca.* 0.051 Å^{-1}, left-hand side of the asymmetric peak), indicating a difference in the characteristic droplet size between the empty and the PIDT-TDQ loaded system, complementing the results from DLS and EPR methods, and inter-droplet (repulsive) interactions.

However, as the scope of the present study was not the exhaustive examination of the structure of the system, we focused on how the polymers affected the size and the interfacial properties of the surfactant layer of the system.

3.6 Viscosity measurements

Rheological behavior of O/W microemulsions was investigated by measuring the viscosity of empty and loaded samples. Low viscosity is essential because when these nanoformulated systems are employed in various applications their administration is facilitated. In the present study, viscosity measurements of empty and loaded microemulsions were performed at 25 °C and 37 °C and the results are summarized in Table 3. As it was observed, viscosity in all cases remained in low range values, indicating the suitability of the developed microemulsions for biomedical applications. The addition of PBDT-DPP did not alter the viscosity of the final system; however, the encapsulation of PIDT-DPP

Table 3 Viscosity measurements in empty and loaded microemulsions

Sample	mPa s at 25 °C	mPa s at 37 °C
Limonene	2.10 ± 0.32	1.85 ± 0.23
Limonene PBDT-DPP	3.36 ± 0.13	3.23 ± 0.07
Limonene PIDT-TDQ	4.45 ± 0.02	4.82 ± 0.12
Empty	3.68 ± 0.15	3.76 ± 0.14
Loaded PBDT-DPP	3.64 ± 0.34	3.81 ± 0.11
Loaded PIDT-TDQ	5.52 ± 0.39	6.03 ± 0.05

increased the overall viscosity indicating the polymer's effect on the rheological properties of the system. As in the case of DLS, the increased concentration of PIDT-TDQ probably affected the properties of the final system. Those alterations are based on the polymer's properties which also increased drastically the viscosity of limonene after its addition. A drastic alteration in the viscosity of the dispersed phase is able to provoke alterations in the diameter and shape of the micelles of the overall structural study.

3.7 Optical properties

The absorption spectra of the PBDT-DPP and PIDT-TDQ O/W microemulsions are presented in Fig. 6. All polymers display a qualitatively similar spectral shape and identical to those in THF solution. For each O/W microemulsion, two major absorption bands are observed.

The PBDT-DPP O/W microemulsion still absorbs in the NIR with a maximum peak at 765 nm, while the PIDT-TDQ O/W microemulsion shows absorption that extends in the SWIR region with a maximum peak at 1023 nm. The absorption maxima of the O/W microemulsions are red shifted *versus* the pristine polymers in THF solution indicating an efficient π–π stacking of the polymer chains when passing from solution to the O/W microemulsion environment.

3.8 Cell viability assay

Cell viability assessment was performed using the MTT assay, a photo-spectrometric sensitive method for quantification of viable cells. In order to determine the effect of microemulsions as nanocarriers and also the effect of π-conjugated polymers as optical bioimaging agents in a wide range of cancer types, different cell lines were selected. More specifically, various human cancer cell lines were tested, namely, skin melanoma cells (WM 164), the human liver cancer cell line (Hep-G2), human nasal epithelial cells (RPMI 2650), the human colon cancer cell line (HTC 116) and the human prostate cancer cell line (PC-3). The choice of the cell lines was made according to their localization in internal organs and organs in direct contact with the external environment. This could ensure the biocompatibility of the developed system and its potential to deliver the novel polymers in different targets. In more detail,

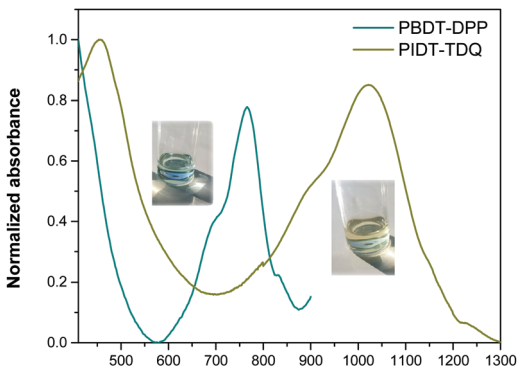

Fig. 6 UV-Vis spectra of the PBDT-DPP and PIDT-TDQ O/W microemulsions.

WM164 and RPMI 2650 were chosen as they represent cancer cells that are observed in organs which are in contact with the external environment such as skin and the nasal septum respectively. In addition, PC-3 cells, Hep-G2 and HCT 116 are observed in internal organs. In all cases, cells were treated with empty microemulsions which were administered into the cell culture medium at a range ratio of 0.1% to 1% v/v, to scan within this range the cytotoxicity of the nanocarrier. Likewise, cells were treated with microemulsions loaded with PBDT-DPP and PIDT-TDQ, which were administered into the cell culture at the same range ratio as empty nanocarriers. The percentage of cell viability was determined at 72 h after treatment onset and the results are shown in Fig. 7 (the culture medium of each line was used as a positive control sample in all cases). The mean (±SD) of two independent experiments, each performed in six replicates, is presented.

As observed, empty microemulsions at a final ratio of 0.1–0.2% v/v in the culture medium (depending on the sensitivity of each cell line) did not affect cell viability.[35,40] In contrast, when the final ratio was higher than 0.2% v/v, cell viability was significantly decreased in all cases. Most probably, the presence of high surfactant concentration in the culture media affected the viability of the cells. However, Span 80 and Labrasol® are generally recognized as safe and are used in food, cosmetic and pharmaceutical products. Interestingly, RPMI 2650 showed greater resistance to increased surfactant concentrations compared to other cell lines. In contrast, the WM164 cell line was the most sensitive to the systems indicating that the system is not appropriate for possible future percutaneous applications.

To assess the effect of the encapsulated polymers, PBDT-DPP and PIDT-TDQ loaded microemulsions were added to the cell cultures at the same concentrations. The effect of loaded microemulsions did not alter the response of cells compared to empty microemulsions at the same volume ratio. At 0.1% v/v of the microemulsion in the culture media, the cell viability percentage was not altered for both empty and loaded microemulsions. These data indicate that the presence of π-conjugated polymers did not inhibit cell proliferation in any of the tested cell lines *in vitro* and can be safely used to study their properties as photoacoustic contrast agents. However, the microemulsion system plays a crucial role and the ingredients must be chosen with caution regarding the application. Importantly, the encapsulation of π-conjugated polymers in the oil cores of the microemulsions did not furtherly affect cell viability. This is in accordance with published results on conjugated polymer nanoaggregates exhibiting low cytotoxicity.[41] Overall, the proposed O/W microemulsions as carriers of the lipophilic conjugated polymers are promising vesicles to deliver the NIR and SWIR absorbing PBDT-DPP and PIDT-TDQ for *in vivo* studies.

3.9 Photoacoustic properties

Consequently, it was of interest to assess whether the microemulsion matrix influenced the photoacoustic signal of the polymers. Photoacoustic amplitudes (PA) for PBDT-DPP and PIDT-TDQ both in limonene and as O/W microemulsions were measured at wavelengths ranging from 680 to 970 nm (Fig. 8).

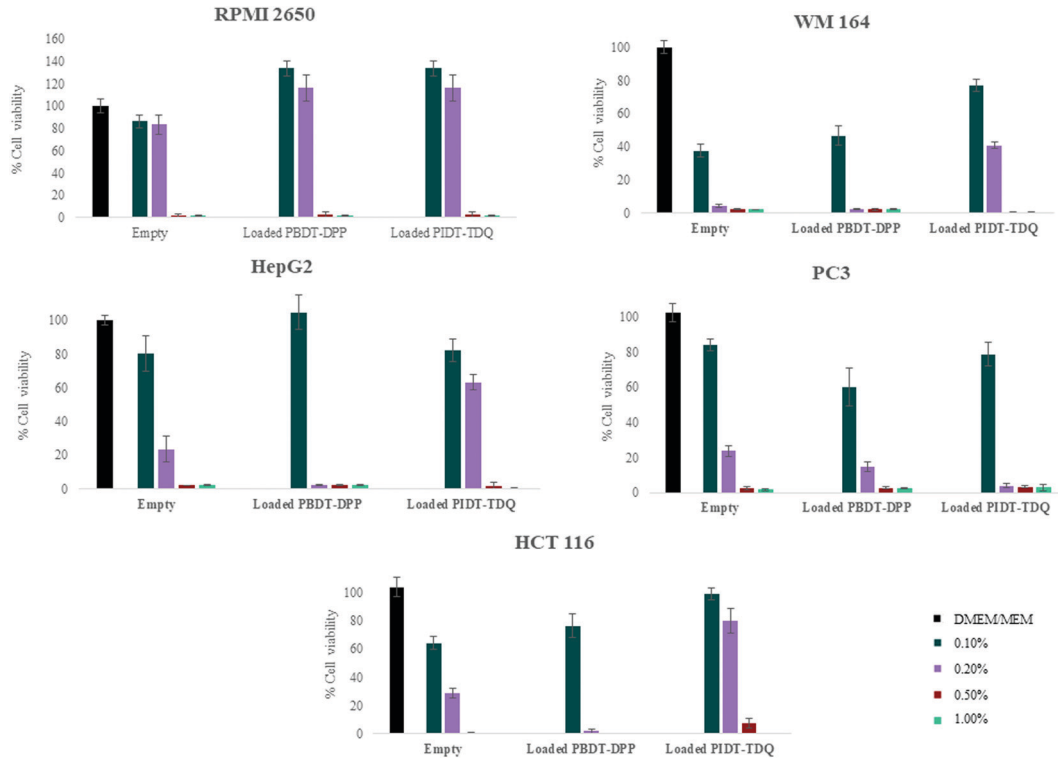

Fig. 7 Effect of empty and loaded systems on the viability of different cell lines after 72 h of exposure using the MTT assay. Each column represents the mean ± SD. Four different concentrations of empty and loaded microemulsions were used: 0.1%, 0.2%, 0.5% and 1% v/v in the culture media.

Between the two conjugated polymers in limonene, it is obvious that PBDT-DPP exhibits a stronger photoacoustic signal *versus* PIDT-TDQ, especially in the 775–875 nm wavelength region. However, the PIDT-TDQ O/W system shows a slightly increased photoacoustic signal with the maximum close to 950 nm as compared to the PBDT-DPP O/W system that shows no obvious photoacoustic signal as determined in the phantom test. As the microemulsion matrix is the same for both polymers it can be assumed that the weak photoacoustic response is attributed to the concentration of the loaded polymers. In addition, it has to be mentioned that the microemulsion's oil phase has been saturated in both cases with PBDT-DPP and PIDT-TDQ polymers respectively and for that reason concentration dependent PA experiments were not feasible. However, the low PA signal is not a prohibitive factor for *in vivo* experiments as the topical biological fluid content may be high enough to have an increased polymer concentration. It has been recently reported that nanoparticles containing the PCPDTBT polymer encapsulated in the PEG2kDa–PLGA4kDa amphiphilic polymer showed a much steeper increase in the signal with increasing dose.[42] Therefore, more studies are underway in order to increase the concentration of the loaded conjugated polymer in the O/W system.

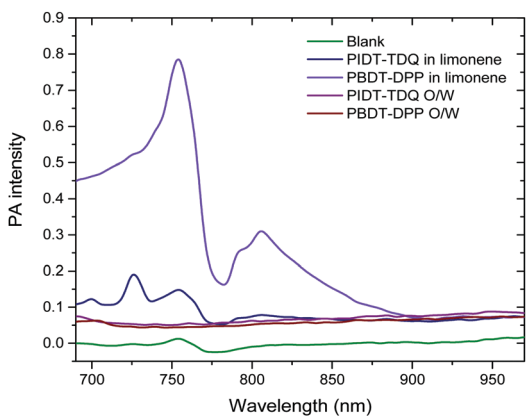

Fig. 8 PA spectra of oil and O/W microemulsions: 1.5 μg mL^{-1} for PBDT-DPP and 7.9 μg mL^{-1} for PIDT-TDQ.

Microemulsions have served as carriers for a variety of compounds from antioxidants to enzymes and antiproliferative agents. In the present study, the strategy of NIR and SWIR polymers' encapsulation was reported for the first time including both structural and activity evaluation methods. Overall, both DLS and SAXS revealed the alteration of the microemulsion's dispersed phase upon the addition of PIDT-TDQ in contrast to the NIR polymer. However, EPR results ruled out the possibility of any substantial polymer–surfactant membrane interaction. The above structural study leads to the conclusion that the increased polymer concentration was the catalytic factor for the final reported photoacoustic properties. In contrast, the polymers' restriction in the oil phase greatly reduced their photoacoustic signal in both cases. The results of this work present the inextricable link between structural and efficacy studies of an encapsulated macromolecule with photoacoustic properties which must necessarily be framed by biological

studies. In the present study, cell viability assay was used in order to point out that the developed systems are suitable for further *in vitro* studies in a wide range of cancer cell lines and further *in vivo* experiments with respect to different cancer types (liver, colon, prostate cancer, *etc.*). However, we cannot predict the pharmacokinetic profile of the proposed systems due to the biological interference and the ADME (Absorption, Distribution, Metabolism and Elimination) properties. The rational use of structural techniques, combining scattering, spectroscopic and microscopic techniques when applicable, can be the cornerstone of preliminary research studies for efficient final carriers. Especially in cases where a plethora of molecules are under investigation the structural study can be the first stage of choice, acting as a screening step for those promising carriers.

4. Conclusions

To summarize, we report the efficient formulation of SWIR and NIR conjugated polymers encapsulated in O/W microemulsions for the first time. This approach enables the simplicity of solubilizing the pre-designed and synthesized conjugated polymers in natural oils and then the formation of the O/W microemulsion with the use of stabilizers. By the use of natural oils, we prevent the utilization of amphiphilic synthetic copolymers which add chemical complexity. The formulated conjugated polymer O/W microemulsions were structurally characterized with a plethora of techniques and it was found that the π-conjugated polymers are located within the oily cores of the microemulsions and not interacting with the surfactant layer at any depth. Furthermore, the viscosity of the O/W microemulsion was low and *in vitro* cell viability studies on various human cancer cell lines such as WM 164, Hep-G2, RPMI 2650, HTC 116 and PC-3 revealed that upon incubation with the O/W microemulsions cell viability was kept high at low concentrations.

Both the physicochemical characteristics and the *in vitro* profile of the systems make them appropriate carriers for compounds associated with pharmaceutical applications from drugs to imaging tools suitable for treatment and diagnosis. Microemulsions are able to penetrate biological barriers with minimum cytotoxicity, while increasing effectively the bioavailability of the encapsulated agent. As a proof-of-concept we have demonstrated that the SWIR absorbing conjugated polymer O/W microemulsion showed photoacoustic response besides the low concentration of the loaded conjugated polymers and for this reason further studies are needed in order to fully exploit these new types of photoacoustic contrast agents for further *in vivo* bioimaging studies. Systems with an increased oil phase concentration will be further studied in order to ensure higher concentrations of π-conjugated polymers while maintaining the carrier's biocompatibility for final increased photoacoustic efficiency. Overall, the proposed microemulsions are proven promising to serve as tools for the delivery of lipophilic π-conjugated polymers for bioimaging applications in various tissues. Such systems combine size at nanoscale, low viscosity, biocompatibility and ability to deliver efficiently highly lipophilic compounds *in vitro*, without affecting their photoacoustic properties. In this context, microemulsions could contribute to overcoming restrictions associated to administration of lipophilic contrast agents for bioimaging, such as π-conjugated polymers.

Funding sources

This work was funded by the Helmholtz European partnering program for the cooperation between German Cancer Research Center (DKFZ) and National Hellenic Research Foundation (NHRF) to build the Athens Comprehensive Cancer Center (ACCC).

Conflicts of interest

There are no conflicts to declare.

Acknowledgements

We would like to thank Dr Christos Chochos and Dr Panagiota Koralli from the Institute of Chemical Biology at National Hellenic Research Foundation for providing the polymer samples and Prof. Dr Antonia Dimitrakopoulou-Strauss and Dr Alkmini Nega from the Clinical Cooperation Unit Nuclear Medicine of the German Cancer Research Center for screening the photoacoustic behavior of the O/W systems. We also thank M. A. Bentaleb for his assistance in the SAXS experiments at CRPP and Dr Fabio Sonvico (University of Parma, Parma, Italy) for providing the RPMI 2650 cell line.

References

1 R. Weissleder and M. J. Pittet, *Nature*, 2008, **452**, 580–589.
2 E. Hemmer, A. Benayas, F. Légaré and F. Vetrone, *Nanoscale Horiz.*, 2016, **1**, 168–184.
3 S. He, J. Song, J. Qu and Z. Cheng, *Chem. Soc. Rev.*, 2018, **47**, 4258–4278.
4 G. Hong, A. L. Antaris and H. Dai, *Nat. Biomed. Eng.*, 2017, **1**, 1–22.
5 K. Pu, A. J. Shuhendler, J. V. Jokerst, J. Mei, S. S. Gambhir, Z. Bao and J. Rao, *Nat. Nanotechnol.*, 2014, **9**, 233–239.
6 C. Wu and D. T. Chiu, Highly Fluorescent Semiconducting Polymer Dots for Biology and Medicine, *Angew. Chem., Int. Ed.*, 2013, **52**, 3086–3109.
7 Y. Lyu, J. Zeng, Y. Jiang, X. Zhen, T. Wang, S. Qiu, X. Lou, M. Gao and K. Pu, *ACS Nano*, 2018, **12**, 1801–1810.
8 D. Tuncel and H. V. Demir, *Nanoscale*, 2010, **2**, 484–494.
9 A. J. C. Kuehne, M. C. Gather and J. Sprakel, *Nat. Commun.*, 2012, **3**, 1–7.
10 M. C. Baier, J. Huber and S. Mecking, *J. Am. Chem. Soc.*, 2009, **131**, 14267–14273.
11 J. Li, J. Rao and K. Pu, *Biomaterials*, 2018, **155**, 217–235.
12 A. Spernath and A. Aserin, *Adv. Colloid Interface Sci.*, 2006, **128**, 47–64.

13 M. Fanun, *Curr. Opin. Colloid Interface Sci.*, 2012, **17**, 306–313.
14 S. Gupta and S. P. Moulik, *J. Pharm. Sci.*, 2008, **97**, 22–45.
15 M. de la Hunty, X. Spindler, S. Chadwick, C. Lennard and C. Roux, *Forensic Sci. Int.*, 2014, **244**, 48–55.
16 M. Pourtabrizi, N. Shahtahmassebi, A. Kompany and S. Sharifi, *J. Fluoresc.*, 2018, **28**, 323–336.
17 E. Lémery, S. Briançon, Y. Chevalier, C. Bordes, T. Oddos, A. Gohier and M. A. Bolzinger, *Colloids Surf., A*, 2015, **469**, 166–179.
18 C. L. Chochos, R. Singh, M. Kim, N. Gasparini, A. Katsouras, C. Kulshreshtha, V. G. Gregoriou, P. E. Keivanidis, T. Ameri, C. J. Brabec, K. Cho and A. Avgeropoulos, *Adv. Funct. Mater.*, 2016, **26**, 1840–1848.
19 L. Yu, W. K. Chan, Y. Chen and Z. Peng, *Mater. Res. Soc. Symp. Proc.*, 1994, **328**, 63–71.
20 Y. Liang, D. Feng, Y. Wu, S. T. Tsai, G. Li, C. Ray and L. Yu, *J. Am. Chem. Soc.*, 2009, **131**, 7792–7799.
21 H. Li, T. L. Tam, Y. M. Lam, S. G. Mhaisalkar and A. C. Grimsdale, *Org. Lett.*, 2011, **13**, 11–14.
22 M. Fanun, V. Papadimitriou and A. Xenakis, *J. Colloid Interface Sci.*, 2011, **361**, 115–121.
23 P. A. Hassan, S. Rana and G. Verma, *Langmuir*, 2015, **31**, 3–12.
24 J. Berliner, *Spin Labeling: Theory and Applications*, Elsevier Science, 1976, p. 609.
25 I. Nikolic, E. Mitsou, A. Damjanovic, V. Papadimitriou, J. Antic-Stankovic, B. Stanojevic, A. Xenakis and S. Savic, *J. Mol. Liq.*, 2020, **301**, 112479.
26 O. H. Griffith and P. C. Jost, Lipid Spin Labels in Biological Membranes, in *Theory and Applications in Spin Labeling*, Academy Press, New York, 1976, pp. 453–523.
27 J. Roncali, P. Leriche and A. Cravino, *Adv. Mater.*, 2007, **19**, 2045–2060.
28 Q. Li, Y. Guo and Y. Liu, *Chem. Mater.*, 2019, **31**, 6359–6379.
29 B. Carsten, F. He, H. J. Son, T. Xu and L. Yu, *Chem. Rev.*, 2011, **3**, 1493–1528.
30 D. Waysbort, S. Ezrahi, A. Aserin, R. Givati and N. Garti, *J. Colloid Interface Sci.*, 1997, **188**, 282–295.
31 A. Khoshnood, B. Lukanov and A. Firoozabadi, *Langmuir*, 2016, **32**, 2175–2183.
32 B. Lindman, U. Olsson and O. Soderman, *Handb. Microemulsion Sci. Technol.*, Routledge, 2018, pp. 309–356.
33 W. Brown, R. Rymdén, J. Van Stam, M. Almgren and G. Svensk, *J. Phys. Chem.*, 1989, **93**, 2512–2519.
34 N. T. Southall, K. A. Dill and A. D. J. Haymet, *J. Phys. Chem. B*, 2002, **106**, 521–533.
35 I. Theochari, M. Goulielmaki, D. Danino, V. Papadimitriou, A. Pintzas and A. Xenakis, *Colloids Surf., B*, 2017, **154**, 350–356.
36 V. Savić, M. Todosijević, T. Ilić, M. Lukić, E. Mitsou, V. Papadimitriou, S. Avramiotis, B. Marković, N. Cekić and S. Savić, *Int. J. Pharm.*, 2017, **529**, 491–505.
37 I. Golfomitsou, E. Mitsou, A. Xenakis and V. Papadimitriou, *J. Mol. Liq.*, 2018, **268**, 734–742.
38 J. Qi, J. Zhuang, W. Wu, Y. Lu, Y. Song, Z. Zhang, J. Jia and Q. Ping, *Int. J. Nanomed.*, 2011, **6**, 985–991.
39 T. N. Zemb, I. S. Barnes, P. J. Derian and B. W. Ninha, Progress in Colloid & Polymer Science, in *Trends in Colloid and Interface Science IV*, ed. M. Zulauf, P. Lindner and P. Terech, 1990, **81**, pp. 20–29.
40 I. Theochari, V. Papadimitriou, D. Papahatjis, N. Assimomytis, E. Pappou, H. Pratsinis, A. Xenakis and V. Pletsa, *Biomimetics*, 2018, **3**, 1–18.
41 H. Tang, C. Xing, L. Liu, Q. Yang and S. Wang, *Small*, 2011, **7**, 1464–1470.
42 T. F. Abelha, P. R. Neumann, J. Holthof, C. A. Dreiss, C. Alexander, M. Green and L. A. Dailey, *J. Mater. Chem. B*, 2019, **7**, 5115–5124.

